Journal of Geochemical Exploration 198 (2019) 1–17

Contents lists available at ScienceDirect

Journal of Geochemical Exploration

journal homepage: www.elsevier.com/locate/gexplo

Impact of heterogeneities and surface roughness on pXRF, pIR, XRD and Raman analyses: Challenges for on-line, real-time combined mineralogical and chemical analyses on drill cores and implication for "high speed" Ni-laterite exploration

Cédric Duée[a,*], Beate Orberger[b,c], Nicolas Maubec[a], Valérie Laperche[a], Laure Capar[a], Anne Bourguignon[a], Xavier Bourrat[a], Yassine El Mendili[d], Daniel Chateigner[d], Stéphanie Gascoin[d], Monique Le Guen[e], Céline Rodriguez[e], Fabien Trotet[e], Mohamed Kadar[e], Karen Devaux[e], Michaël Ollier[e], Henry Pillière[f], Thomas Lefèvre[f], Dominique Harang[f], Fons Eijkelkamp[g], Harm Nolte[g], Peter Koert[g]

[a] BRGM, F-45060 Orléans, France
[b] GEOPS, Université Paris Sud, Université Paris Saclay, Bât 504, 91405 Orsay, Cedex, France
[c] CATURA Geoprojects, 7 rue Ernest Pischari, 75007 Paris, France
[d] CRISMAT-ENSICAEN, UMR CNRS 6508, Normandie Université, 6 boulevard Maréchal Juin, 14050 Caen, France
[e] ERAMET SA-ER-SLN, 1 Avenue Albert Einstein, 78190 Trappes, France
[f] Thermo Fisher Scientific, 71 rue d'Orléans, 45410 Artenay, France
[g] Eijkelkamp SonicSampDrill, Uitmaat 8, 6987 ER Giesbeek, the Netherlands

ARTICLE INFO

Keywords:
Portable instruments
Drill cores
Surface effects
Nickel
Garnierite

ABSTRACT

On-line, real-time chemical and mineralogical analyses on drill cores are highly demanded by mining companies. However, they are a challenge because of drill core surface state and sample heterogeneities. We selected four rock samples: highly porous, siliceous breccia and serpentinized harzburgite coming from the base of a nickel laterite profile in New Caledonia which were sonic drilled, and fine grained, homogeneous sandstone and coarse grained granite which were diamond drilled and provided by Eijkelkamp Sonic Drill with unknown origin. The samples were analysed at five surface states (diamond or sonic drilled, cut as squares, polished at 6 and 0.25 μm, powdered < 80 μm) by portable XRF spectroscopy (pXRF) in mining and soil modes and portable infrared spectroscopy (pIR, Visible and Near Infrared-Short Wave Infrared range (VNIR-SWIR)). A total of 52 pXRF and 200 pIR analyses were performed per sample at each surface state. This study shows that the surface state has minor influence on the results of the portable instruments. By comparing pIR and pXRF results with laboratory devices (Raman spectroscopy, XRD with Rietveld refinement, XRF spectroscopy and ICP-AES), we evidence the lower and less accurate information obtained from handheld instruments in terms of chemistry and mineralogy. The porosity and grain size effect on the measurement need to be taken into consideration for on-line drill core analyses. We show that the combination of complementary analytical techniques helps to overcome the drawbacks of the core texture and of the precision of portable instruments in order to define the regions of interest (ROI) for mining companies. We also demonstrate that a precise pXRF calibration is mandatory and that the concentration of light elements (Si, Mg), even if not accurate, shows sufficient contrast along the lateritic profile for ROI definition.

1. Introduction

Combined on-line mineralogical and chemical analyses represent a challenge for the companies designing and constructing the instruments, as the industrial and/or academic end-user needs to achieve reliable data, actionable for exploration, geo-modeling and ore processing. The reliability and representativeness of samples and data, as well as real-time analyses and close-to-real-time decision making will

* Corresponding author.
E-mail address: c.duee@brgm.fr (C. Duée).

https://doi.org/10.1016/j.gexplo.2018.12.010
Received 12 April 2018; Received in revised form 16 November 2018; Accepted 9 December 2018
Available online 13 December 2018
0375-6742/

significantly contribute to continuous updating of the geo-models in the resource and reserve estimate process. While exploration and mining companies perform systematic whole rock chemical analyses, systematic mineralogical analyses are rarely performed. In ore-bearing regolith, such as Ni-Co laterites or bauxites, where multiple metal carriers are present, it is important to record both chemical and mineralogical data systematically to define the metal deportment and the geometallurgical parameters, in order to optimize ore processing and anticipate dysfunction. Combined mineralogical and chemical analyses on drill cores are at present highly demanded by mining and metallurgical companies to speed up all these processes and significantly reduce the operational exploration and processing costs, which represent about 70% of a mining project.

Portable instruments, such as pXRF and VNIR-SWIR pIR spectrometers are widely used on drill cores and outcrops (Portable XRF Services, 2016). pXRF provides semiquantitative chemical analyses, when well calibrated (Hall et al., 2014; Hall et al., 2012). Infra-Red (IR) spectroscopy data provide information on mineralogy, peculiarly on hydrous silicates (e.g. clay minerals), and oxy-hydroxides (e.g. goethite), which are related to alteration halos vectoring mineralization (Chang and Yang, 2012; Duke and Lewis, 2010). Portable VNIR spectroscopy finds also application in heavy metal assessment in polluted soils for pH prediction (Hu et al., 2017). Portable Raman spectroscopy has been recently successfully applied on industrial minerals, e.g. complex intermingled carbonates for the cement industry (Kristova et al., 2013) and on banded iron formations to distinguish Fe-bearing minerals from gangue phases (Wells and Ramanaidou, 2015). These methods give complementary information, they are non-destructive and do not need any sample preparation. They have been used on outcrops, drill core sections, and loose material. However, the studies mentioned above rarely indicate the location and size of the analysed surface area and/or surface state.

Automated imaging–scanning systems (e.g. RGB images analysis) are used for example in the iron ore mining industries to characterize ore textures and to define geometallurgical parameters (Pérez-Barnuevo et al., 2018). They are available on the market (e.g. http://www.dmt-group.com/products/geo-measuring-systems/dmt-corescan.html). At present, one semi-automatized and non-destructive multi sensor system is commercialized by Geotek (http://www.geotek.co.uk/sites/default/files/MSCLOverview.pdf), combining chemical (XRF), mineralogical (VIS-NIR spectroscopy), and colour spectrophotometry, along with P-wave velocity, gamma density, magnetic susceptibility, electrical resistivity, colour line scan imaging, and gamma spectrometry (about 4 m drill core/h, sampling intervals down to 1 mm). It has been tested on a Zn-Cu deposit (Matagami mining camp, Canada, (Ross et al., 2013)).

At present, mineralogical and/or chemical analyses are performed non-simultaneously on-line, but separately by using a single technique, such as hyperspectral imaging or XRF scanner (Cudahy et al., 2009; Gomez Laserna, 2015; Haest et al., 2012; Lypaczewski et al., 2017; Roache et al., 2011; Whitbourn et al., 2011). Operating systems widely used in Australian companies are e.g. the Hy-logger (http://www.csiro.au) or Corescan (www.corescan.com.au). Chemical logging is performed by XRF scanners (e.g. http://www.avaatech.com/; ITRAX XRF). Laser-induced breakdown-spectroscopy (LIBS) for drill cores (Haavisto et al., 2013; Streubel et al., 2016) is recently under development for specific ore types, e.g. lithium, gold and copper mineralizations (Nguegang Kamwa et al., 2017). Many of these techniques are nowadays combined with RGB (red-green-blue) cameras (Braibant et al., 2018). These powerful techniques still need major developments for obtaining reliable analyses.

The SOLSA project (G.A. No. 689868), funded by the EU-H2020 Raw Material program, constructs an expert system coupling sonic drilling with automated analyses of a RGB camera, profilometer, XRF and hyperspectral imaging (VNIR and SWIR) (SOLSA ID A). The containerized and semi-automatized SOLSA ID A system will operate beside SOLSA DRILL targets to analyse up to 80 m drill core per day. Its purpose is to define regions of interests (ROI), which will be further analysed by a combined analytical benchtop system integrating XRF, XRD, Raman and IR spectroscopy (SOLSA ID B) operating off-line close to SOLSA ID A.

SOLSA DRILL and SOLSA IDENTIFICATION (SOLSA ID A + B), comprising the analytical instruments, will be validated for Ni-laterite mines in New Caledonia. The definition of the individual and combined instrumental parameters for on-line, real-time, on-site analyses is tested by portable and laboratory instruments with different configurations. Non-destructive chemical and mineralogical analyses on undestroyed drill cores are problematic as representative sampling is not fully ensured. Particle size distribution, sample heterogeneity, surface states and humidity may influence the results. For example, moisture in and on drill cores impacts e.g. colours and attenuate spectra recorded by hyperspectral cameras (Shankar, 2015).

The influence of surface state on the results was also well demonstrated by the systematic studies with handheld and benchtop XRF instruments (Hall et al., 2011; Hall et al., 2014, 2012; Laperche, 2005; Quiniou and Laperche, 2014; Ross et al., 2014a, 2014b). Spatial dispersion is a measure of both instrument precision and sample heterogeneity. Regarding the accuracy of the chemical and mineralogical results, several parameters have a significant impact like the proximity to surface, humidity, matrix effect, dust, surface roughness (Liritzis and Zacharias, 2011; Shackley, 2010; Tjallingii et al., 2007; Tykot, 2016).

The aim of this paper is to evaluate the impact of physical parameters, such as surface roughness, cracks, porosities and sample heterogeneities on different signals. A cross-method approach was used, combining pIR spectroscopy and pXRF analyses on the same sample areas. Moreover, all samples were analysed by laboratory methods (XRD with Rietveld refinement, Raman Spectroscopy, XRF and ICP-AES). This is the first systematic study of pXRF and pIR analyses on five different surface states of the same samples: (i) drilled (sonic and diamond), (ii) powdered, (iii) cut, (iv) coarse and (v) fine polished. In order to evaluate the impact of heterogeneities, the sample selection is based on the following criteria: similar major mineralogy and chemistry, but different rock textures, porosities (sandstone, SD, siliceous breccia, SB), coarse granular textures of a bright rock (granite, GN) and medium granular dark rock with minerals of similar chemical composition (serpentinized harzburgite, HG). The siliceous breccia and the serpentinized harzburgite are characteristic lithologies occurring at the base of Ni-laterite profiles in New Caledonia (Cathelineau et al., 2017). The serpentinized harzburgite is the bed rock of the Ni-laterite. It hosts locally veins filled with a mixture of different Ni-rich phyllosilicates, also called garnierite (Cathelineau et al., 2017). The siliceous breccia hosts saprolite clasts and was formed later than the Ni-laterite. This study contributes to the definition of instrumental configurations and the analytical conditions of the SOLSA ID A system.

2. Materials and methods

2.1. Sample materials

For this study, we selected four samples.

The first sample is a homogeneous millimetric grain size white beige sandstone (SD; SOLSA label: ER-PG00-0001), with local occurrence of iron oxides. The second sample is a coarse-grained (millimetric to centimetric) grey granite (GN; SOLSA label: ER-UK00-0005). The third sample is a siliceous breccia with millimetric to centimetric pores partly filled with greenish and white talc-like phases. The breccia also hosts saprolite clasts, thus it was formed after lateritisation (SB, SOLSA label: ER-NC00-0001). The last one is a coarse to medium-grained serpentinized harzburgite (HG; SOLSA-label: ER-NC00-0003; Fig. 1).

All samples are coming from drill core material. They are sonic drilled (usually showing no drilling marks on core surface) for SD and GN (provided by Eijkelkamp Sonic Drill with unknown origin), and diamond drilled (usually showing drilling marks on core surface) for SB and HG (provided

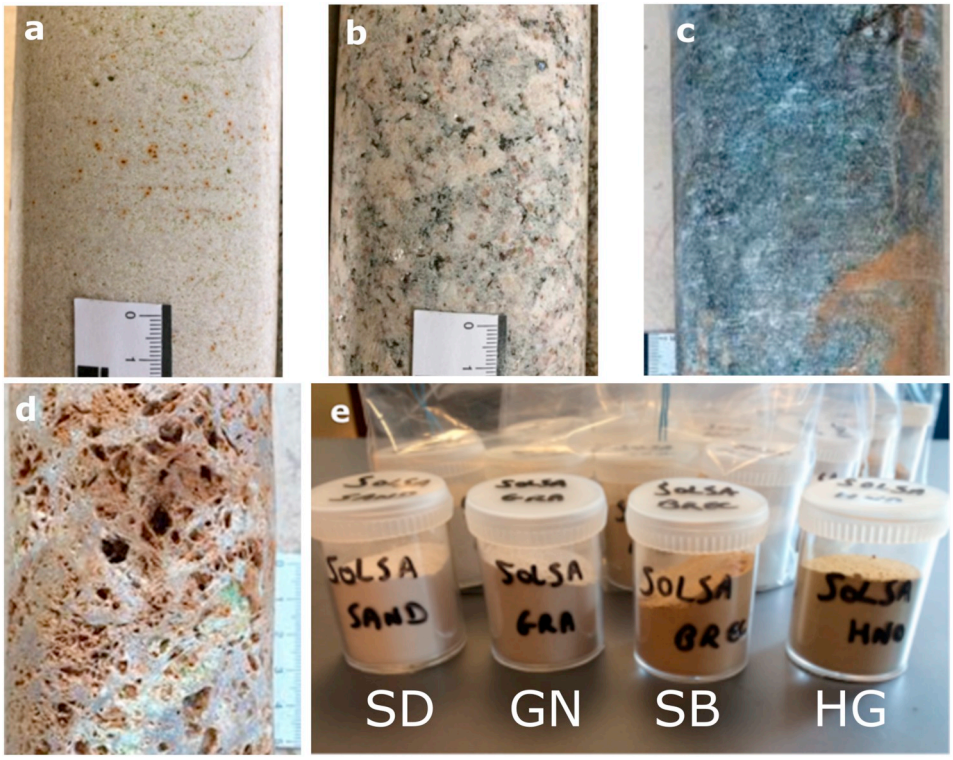

Fig. 1. Studied samples: drill cores (a) Sandstone (SD), (b) Granite (GN), (c) Serpentinized Harzburgite (HG), (d) Siliceous Breccia (SB), and (e) powders.

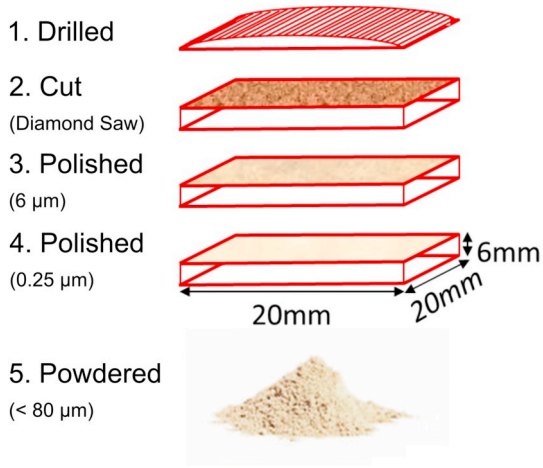

Fig. 2. Scheme of the surface states studied.

by SLN, New Caledonia). Sonic and diamond drilled core parts were cut from the core material (20 × 20 mm^2 squares with a thickness of 6 mm, Fig. 2). The drilling conditions are presented in Table 1. Four types of surface conditions were studied: (a) convex surface as drilled, (b) diamond saw-cut, (c) polished at 6 µm, (d) polished at 0.25 µm. Representative samples were cut off the drill cores, powdered and sieved at 80 µm (Figs. 1 and 2). Additional analyses were performed on the fraction < 80 µm of the sieved samples. In the text, the squares are named bulk samples.

2.2. Methods

2.2.1. Portable X-ray fluorescence spectroscopy

Portable X-ray fluorescence (pXRF) analyses were performed with a Thermo Fisher Scientific NITON XL3t 980 GOLDD model (BRGM) using the mining and the soil modes, with an 8 mm diameter analytical window. Mining and soil modes are two modes offering diverse advantages. The mining mode is expected to offer a better calibration for some elements such as metals, and is more favourable to measure lighter elements (Mg, Al, Si, P, S, Cl). On the contrary, the soil mode is expected to present a better calibration for traces elements, but does not allow detecting lighter elements. We worked with both modes due to the diversity of the selected samples.

This energy dispersive pXRF is fitted with an X-ray tube (max. 50 kV, 100 µA, 2 W) with an Ag anode target excitation source to avoid contamination, and a Large Drift Detector (LDD). The source counting time for the analysis was set at 30 s for each filter, enhancing the detector sensibility for different ranges of elements. The total counting time was 120 s using the 4 filters of the pXRF to analyse light elements such as Si, Al and Mg using the mining mode, and 90 s using 3 filters at the soil mode. In order to obtain statistically reliable data, 26 measurements for each mode were acquired for each solid sample (52 pXRF analyses per sample), and 13 for the powdered samples (26 counting the two modes). The latter represents ideal conditions for representative sampling and homogeneous grain size. The device was calibrated with NIST standards (National Institute of Standards and Technology, https://www.nist.gov/srm). In this paper, the pXRF data

Table 1
Drilling conditions.

Machine	CRS-V (CompactRotoSonic-V)	CoreBarrel length	2 m
Drill head	CompactRotoSonic	Bit type	Rock Ring Bit, front discharge
CoreBarrel type	Dual wall	Bit OD	126 mm
CoreBarrel ID	89 mm	Bit ID	89 mm
CoreBarrel OD	114 mm	Fluid used	Water

are presented in box-and-whisker plots format (Tukey, 1977).

2.2.2. Laboratory XRF and ICP

In addition, laboratory XRF (called thereafter BT-XRF, standing for Benchtop X-Ray Fluorescence) for major and trace elements, and ICP-AES for trace elements, have been performed at BRGM (Orléans, France) in order to compare the results with pXRF. For BT-XRF, after calcination at 1025 °C and addition of lithium tetraborate ($Li_2B_4O_7$), a glass bead was prepared and analysed with a Zetium spectrometer (Panalytical). For ICP-AES analyses, the sample was heated at 450 °C. Then an alkaline sintering with sodium peroxide (Na_2O_2) was performed at 450 °C. The sintered sample was then treated with HCl and analysed with an Arcos ICP-AES spectrometer (Ametek Spectro). These analyses were used for calibration of the pXRF device additionally to that of the NIST. In the figures referring to pXRF results, dashed lines represent laboratory XRF and ICP results. The absence of dashed line for an element indicates that the result was below the detection limits of the laboratory device.

2.2.3. Portable Infra-Red spectroscopy

The reflectance spectra were measured using an ASD FieldSpec Pro FR® portable spectrometer covering the 350–2500 nm spectral range in the electromagnetic spectrum, with a spatial resolution of 10 nm and a 2 nm sampling in the SWIR. A contact probe device, with a viewing area of 2-cm-diameter circle and its own light source, was used. A white Spectralon standard (Labsphere) served as the reflectance standard. We worked in relative reflectance. The spectrum average has been determined by striking a compromise between noise reduction through averaging the spectra and the time desired for each spectrum collection. For this study, an average of 20 measurements with a counting time of 1/10 s per measurement has been chosen. We used the ViewSpec™ utilities to calculate the bias value for the VNIR and SWIR2 regions. This is usually done only for presentations and documentation or when using data to match with a spectral library. It is not meant to correct the data. To optimize the signal-to-noise ratio, the mean spectrum for each sample was computed from ten spectral measurements.

2.2.4. Laboratory Raman spectroscopy

The laboratory Raman experiments were carried out at the Maine University, IMMM, Le Mans, France, using a confocal Horiba Jobin Yvon T64000 spectrometer equipped with a 600-lines mm^{-1} grating (defining the resolution) coupled to a liquid N_2-cooled charge-coupled device detector. Raman spectra were recorded at room temperature in backscattering configuration under a microscope (Olympus BX41) with a 100× objective focusing the 514 nm line from an Ar-Kr ion laser. The spot diameter of the laser was estimated at 0.8 µm for bulk samples and 10 µm for powders at a spectral resolution of 2 cm^{-1}. Raman measurements were carried out at the low laser power of 0.8 mW to avoid thermal modification or degradation of the minerals. Single spectra were recorded twice in the 80–2250 cm^{-1} wavenumber region with an integration time varying between 60 and 100 s. Spectra acquisitions were managed using the LabSpec software.

2.2.5. Laboratory X-ray diffraction

X-ray diffraction was carried out on powdered samples with a Siemens D5000 diffractometer (BRGM; Co-tube, 2θ range from 4° to 84°, with 0.03° step and 13.5 s/point). DIFFRAC Plus EVA software was used for the interpretation of the X-ray diffractograms. Quantitative mineralogy was obtained using Rietveld refinement and the MAUD (Materials Analysis Using Diffraction) software (Lutterotti et al., 1997).

It is worth noting that, since each analytical method has its own area of analysis, no comparison was performed between the techniques, except for laboratory and portable XRF. The aim of using several analytical methods was to ensure a comprehensive study of our samples and to determine the limits of the portable instruments for the SOLSA expert system. Obviously, laboratory instruments (laser spot of 0.8 and 10 µm for Raman for example) have a better resolution than portable instruments (spot of 8 mm and 2 cm diameter for pXRF and pIR, respectively).

3. Results

3.1. Analyses on powdered samples of all lithologies

Powdered samples are considered to have the most homogeneous and representative compositions, and are thus taken as a reference for the analyses performed on the different surface states (drilled, cut, and polished).

The X-ray Diffraction patterns are presented in Fig. 3 along with the results of phase quantification by Rietveld refinement (see also Fig. S1). SD and SB are principally composed of quartz (about 100 wt% quartz in SB in accordance with the results of Secchi et al. (2018)). GN is composed of ~27 wt% quartz, and ~48 wt% of K-feldspars and plagioclase, ~25 wt% of phyllosilicates (Fig. 3). HG is composed of serpentine (57 wt%), forsterite (29 wt%), enstatite (11 wt%), talc (3 wt%) and traces of amphiboles. XRD analyses and Rietveld refinement performed by Secchi et al. (2018) found the same major minerals on HG, but since the analysis was not performed on the exact same piece of sample, slightly different mineral proportions were obtained (77 wt% lizardite, 16 wt% forsterite, 7.7 wt% enstatite).

Laboratory Raman spectroscopy was carried out on all sample powders, detecting essentially quartz and minor feldspar in GN; quartz in SD and SB; and lizardite and forsterite in HG (Fig. 4).

As powders have a brighter colour compared to rock samples, they present a higher reflectance. This is clearly expressed in the VNIR and SWIR regions (Fig. 5). However, the vibration bands in the powder spectra appear less intense that in the case of bulk samples. So, the minerals are difficult to identify directly from the reflectance spectra, but working with the continuum removed spectra was successful. The latter highlights the presence of water molecules in all samples, along with goethite in SB, hematite and illite in GN, serpentine in HG and hematite and illite or montmorillonite in SD (Fig. 5).

Selected pXRF analyses in mining and soil modes are presented in Figs. 6 to 9 (complete results are presented in Figs. S2 to S5). Combining both analysis modes allows detecting more elements than using only one mode (Figs. 6 to 9 and S2 to S5). Since the light filter is not used in soil mode, the spectrometer does not detect Si, Al, Mg, S, Cl or P. However, some trace elements, not detected in the mining mode, are detected using the soil mode (K, Ti, Cd, V, Sb in SB, and K, V and Ba in SD, Figs. 6, 7, S2 and S3). Finally, significant differences arise between pXRF and laboratory values for the same powders, independently of the analysis mode.

Laboratory chemical analyses (BT-XRF, ICP-AES) of SD show coherent values for Fe and Zr in both pXRF modes (Fe: 127–239 ppm in mining mode and 137–238 ppm in soil mode; Zr: 52–78 ppm in mining mode and 68–107 ppm in soil mode, in comparison with 210 ppm and 113 ppm for laboratory measurements, respectively), and for Ti in soil mode (380–477 ppm versus 400 ppm by ICP). However, the pXRF values for Si (39.5–43.0%), Sr (1.7–3.5 ppm in mining mode and 3.6–6.2 ppm in soil mode) and Ti in mining mode (232–271 ppm) are different from those obtained in laboratory (45.5%, 19 ppm and 400 ppm, respectively) (Figs. 6 and S2). For SB, the laboratory values are around the detection limits and differ from those obtained by pXRF for almost all elements (e.g. a factor 2 for Fe and Mn in soil mode) except for Cr in soil mode (around 990 ppm versus 880 ppm by ICP) (Figs. 7 and S3). GN analyses also differ between laboratory and pXRF values, up to a factor 4 for Ba in soil mode (49–108 ppm versus 385 ppm by ICP), and 4% for Si (28.8–30.6% versus 33.1% by XRF) (Figs. 8 and S4). Finally, HG shows significant differences between laboratory and portable measurements, up to 13% for Mg (24.5% versus 10.1–11.6%, respectively) (Figs. 9 and S5).

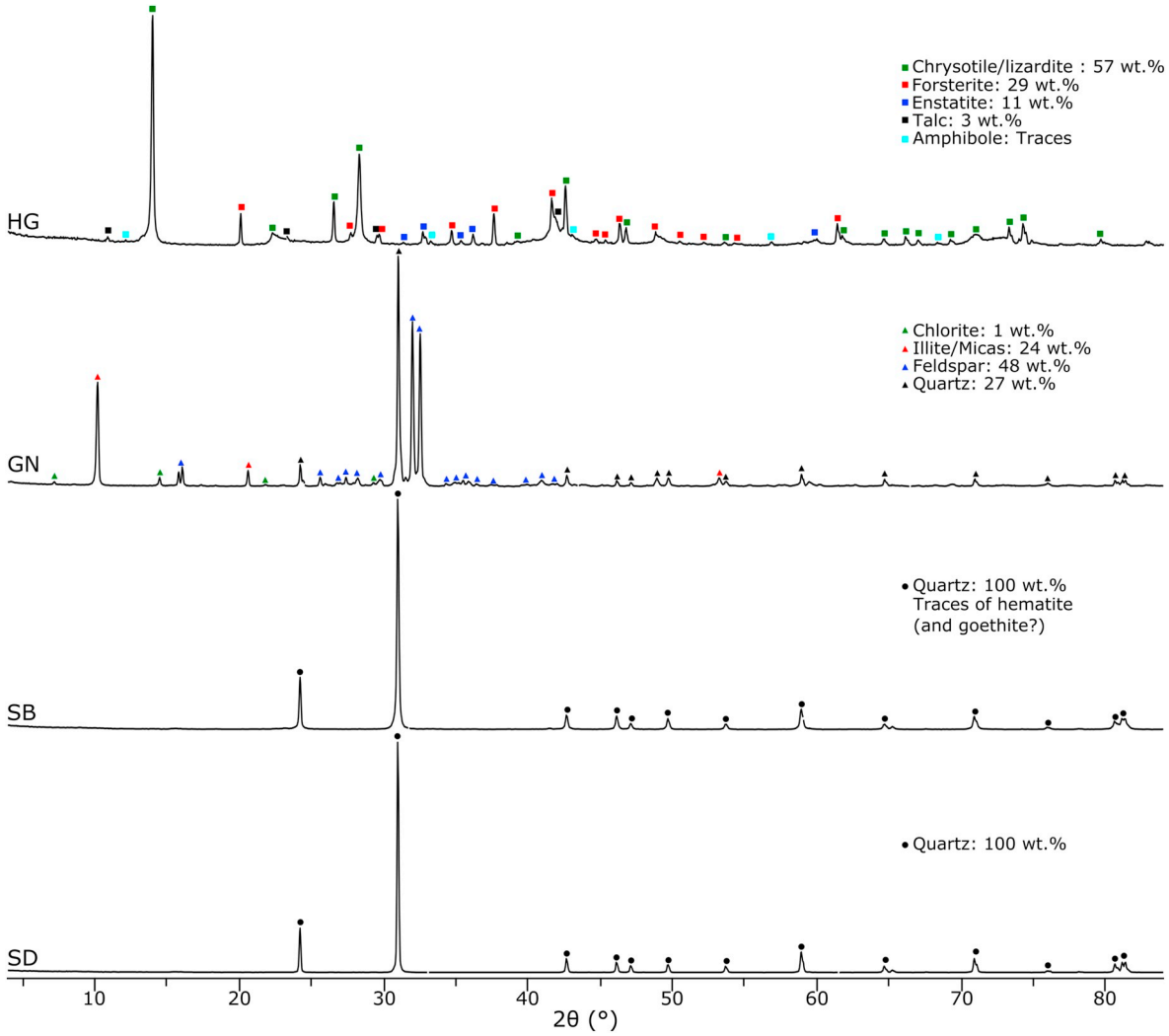

Fig. 3. X-ray diffractograms for the four powders and quantification of the phases obtained from Rietveld refinement.

3.2. Analyses on bulk samples

3.2.1. Sandstone (SD)

The pIR analyses performed on SD show that polishing slightly decreases the reflectance and slightly increases the peak intensity (Fig. 5). The presence of bound water (~1400 and 1900 nm), illite or montmorillonite (2200 nm) is evidenced (Fig. 5). Quartz cannot be detected by pIR as characteristic peaks only appear in the Thermal Infra-Red (TIR) region (~9000 nm) (Clark, 1999). However, it is confirmed by micro-Raman spectroscopy (Fig. 10). Furthermore, traces of anatase (TiO_2), kaolinite ($Al_2Si_2O_5(OH)_4$), pyrite (FeS_2), hematite (Fe_2O_3), maghemite (γ-Fe_2O_3), goethite (FeO(OH)) and zircon ($ZrSiO_4$) were detected (Fig. 10).

The pXRF analyses are rather coherent for the four surface states in both modes, except for Si (45.4–50.1 wt% versus 51.4–54.8 wt%), Ca (153–768 ppm versus 107–191 ppm in soil mode) and Fe (117–722 ppm versus 58–203 ppm in mining mode) in the drilled samples (Figs. 6 and S2). This is probably related to the surface roughness of the drilled samples in comparison to the polished samples. Local anomalous high concentrations (e.g. Ti and Zr) in bulk samples are related to the presence of anatase (TiO_2) and zircon ($ZrSiO_4$).

Working in both mining and soil modes enhance the number of elements detected (11). In comparison with XRF and ICP laboratory values, pXRF shows highly variable results for Si, Sr, and Ti (Figs. 6 and S2).

3.2.2. Siliceous breccia (SB)

With pIR, water molecules are identified at 1420 and 1920 nm. The band at 500 nm may correspond to goethite (Fig. 5). Micro-Raman spectroscopy confirms quartz as the major phase, and the presence of hematite (Fe_2O_3) and goethite (α-FeO(OH)). Furthermore, hedenbergite ($CaFeSiO_3$), olivine (forsterite Mg_2SiO_4 according to XRD), calcite ($CaCO_3$), magnetite (Fe_3O_4) and maghemite (γ-Fe_2O_3) were detected (Fig. 10). Raman spectroscopy performed with 633 and 785 nm laser wavelengths on a rough surface of a different piece of SB sample detected additionally moganite, a SiO_2 polymorph (Secchi et al., 2018).

SB shows highly variable pXRF analyses for almost all elements in the different surface states (Figs. 7 and S3), related to variable and high porosities (Fig. 1d), variable porosity fillings (garnierite and other phyllosilicates), and the presence of lithoclasts composed of forsterite, hedenbergite and serpentine. Moreover, in both modes, Ni is detected up to 0.7 wt% (Figs. 7 and S3).

When comparing portable and laboratory values, similar observations are made as for sandstone, i.e. an overestimation of Si (50 wt% instead of 37 wt%) and Mg (0.75 wt% versus 0.4 wt%) by pXRF. On the contrary, results obtained by pXRF for Ni, Fe and Cr are lower than laboratory results (Figs. 7 and S3).

3.2.3. Granite (GN)

Portable IR shows the presence of bound water (1400 and 1900 nm) and illite (2200, 2347 and 2440 nm) (Fig. 5).

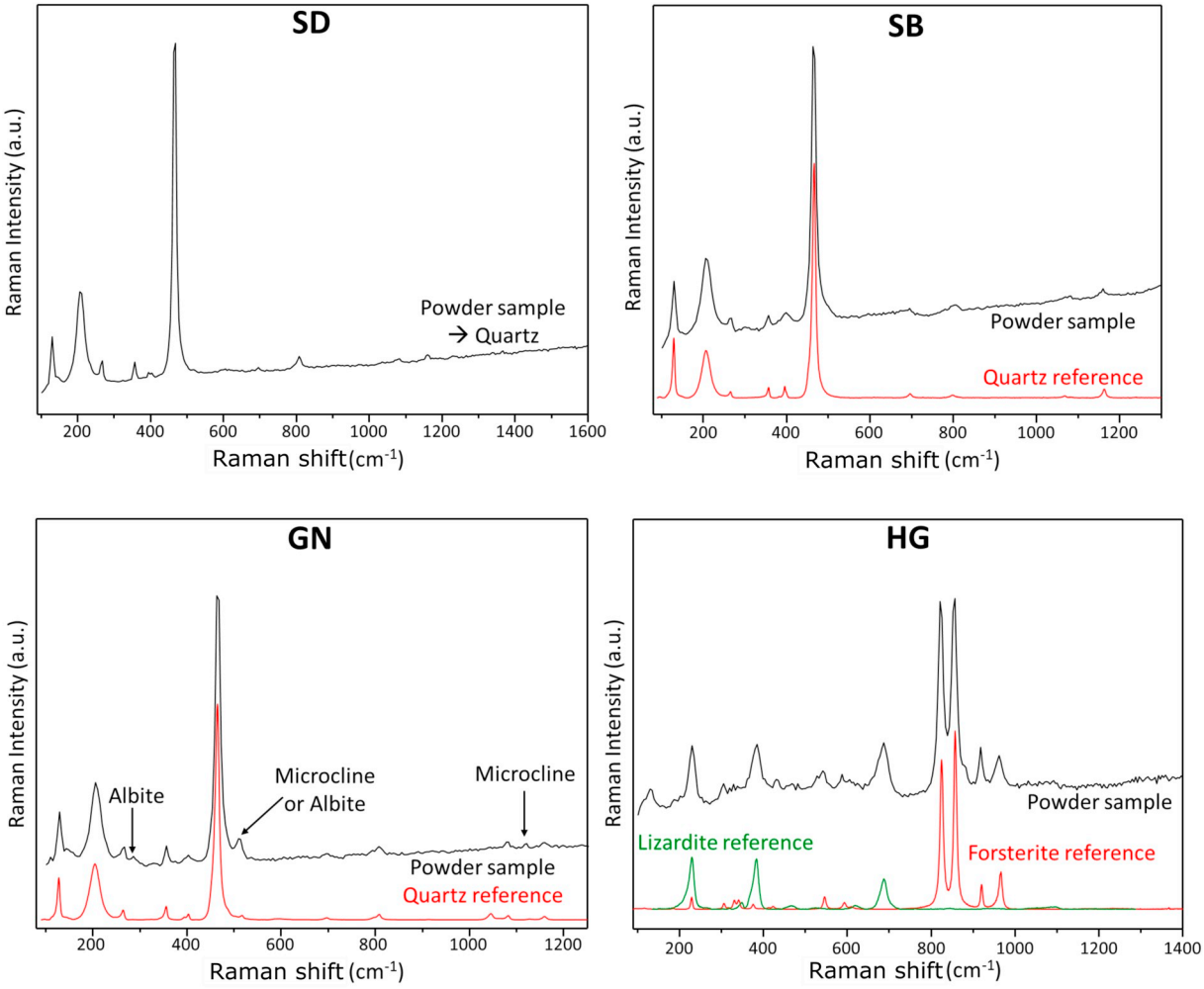

Fig. 4. Raman spectra of the four powders.

Micro-Raman spectroscopy confirms the presence of quartz, albite, biotite, microcline and mica (muscovite $KAl_2(AlSi_3O_{10})(F,OH)_2$), and detects additionally the presence of kaolinite ($Al_2Si_2O_5(OH)_4$), gypsum ($CaSO_4{\cdot}2H_2O$), magnesium sulphate ($MgSO_4$), rutile (TiO_2), anatase (TiO_2), calcite ($CaCO_3$) and hematite (Fe_2O_3) (Fig. 10).

Portable XRF detects 23 elements using both modes (Figs. 8 and S4). Tellurium was detected in soil mode (around 60 ppm), but such a large amount is unlikely in this granite. The Kα and Kβ peaks of Te arise at the same energy than those of Ca (4.01 and 3.7 keV) and the latter was measured at about 0.5 wt% by laboratory XRF. Independently on the surface state, similar scatterings are observed for all elements (Figs. 8 and S4). Si, Mg, Cr, Sn and V are overestimated by pXRF compared to laboratory results, while Sr and Zr are underestimated.

3.2.4. Serpentinized harzburgite (HG)

Portable IR on the dark green rock shows weak reflectance and detects serpentine. Polishing decreases the reflectance and slightly enhances the peak intensity (Fig. 5). Micro-Raman spectroscopy specifies that the major serpentine mineral is lizardite ($(Mg)_3Si_2O_5(OH)_4$), confirms the presence of both forsterite (Mg_2SiO_4) and enstatite ($MgSiO_3$), and, additionally, detects quartz (SiO_2), anatase (TiO_2), rutile (TiO_2), pyrite (FeS_2), talc ($Mg_3Si_4O_{10}(OH)_2$), magnesiochromite ($MgCr_2O_4$), cowlesite ($CaAl_2Si_3O_{10}{\cdot}6(H_2O)$), magnetite ($Fe_3O_4$), maghemite ($\gamma$-$Fe_2O_3$), hematite ($Fe_2O_3$) and goethite ($FeO(OH)$) (Fig. 10).

HG, with a less contrasting mineralogy (all minerals host Mg, Fe and Si) than granite or breccia, shows less variable pXRF results for all surface states (Figs. 9 and S5). This is similar to SD (Figs. 6 and S2). However, portable and laboratory measurements differ for Si, Al, Fe in mining mode and Mn in soil mode. They are overestimated, while Mg and Ni (~0.2 wt%) are underestimated when analysed with pXRF. Tin detected in soil mode at around 30 ppm, needs to be confirmed by laboratory XRF analysis.

4. Discussion

The SOLSA expert system will be composed of SOLSA drill, an on-line real-time analytical system, and an on-mine combined analytical benchtop system. In order to propose an approach similar to this system, we tested portable and laboratory instruments on different surface roughness on homogeneous and heterogeneous samples of different mineralogy and chemistry.

4.1. Surface state and heterogeneity of the samples

Our study showed that the surface state of the sample does not have a significant influence on the pIR spectra (Fig. 5). However, the pIR signal is affected by the reflectance of the material. Powders have brighter colour than the corresponding bulk samples (see Fig. 1) and thus present higher reflectance than bulk samples. Similarly, dark bulk samples such as serpentinized harzburgite, have lower reflectance than bright samples, such as sandstone and breccia (Fig. 5). As Ni-laterites exhibit essentially dark colours, such as green, brown, yellow brown and reddish from bottom to top of the drilled core, the light source must be particularly adapted to such materials, to reach optimal reflectance

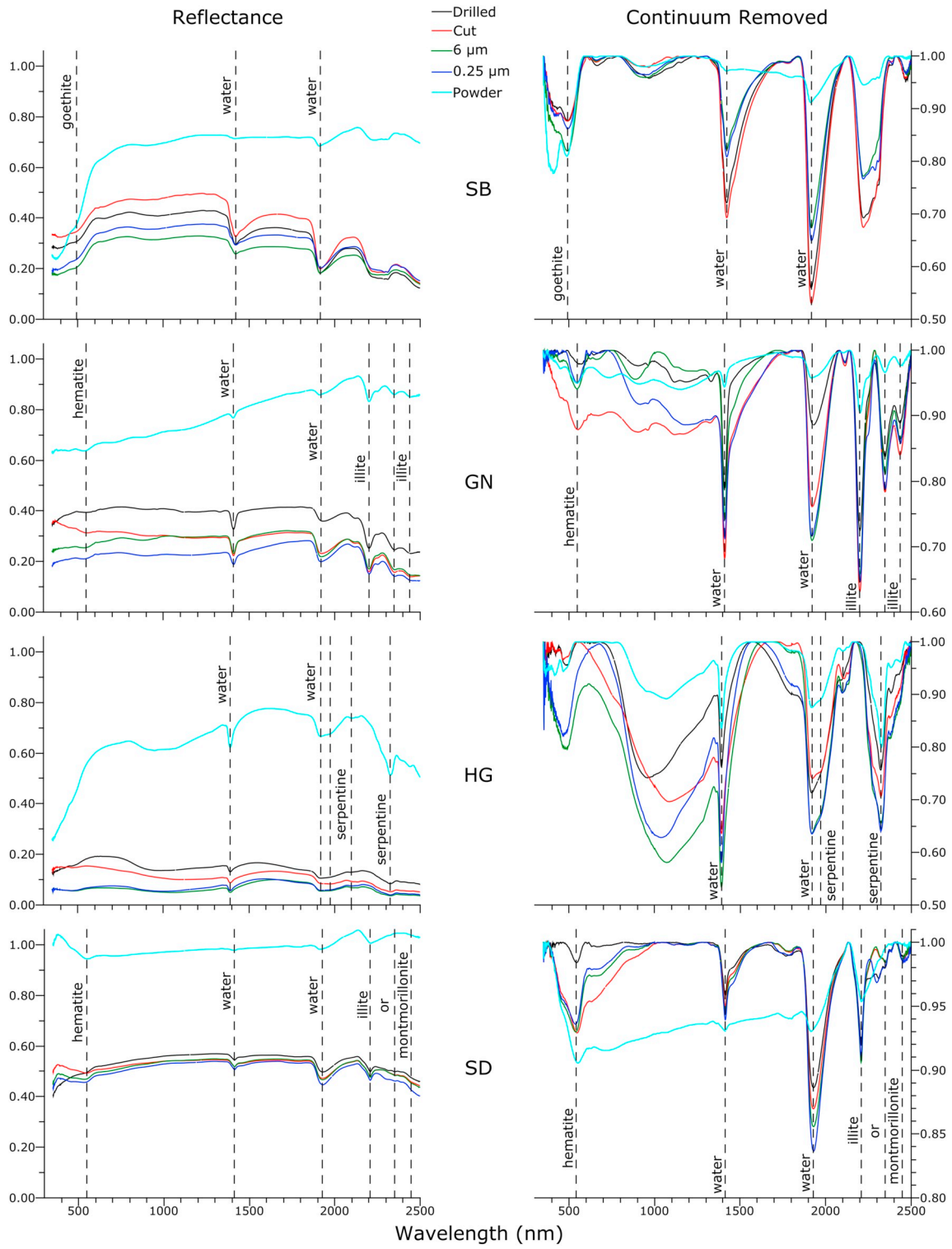

Fig. 5. Portable IR spectra. Left: Reflectance spectra. Right: Continuum removed spectra.

without shadow zones. Furthermore, the laterite horizons contain metastable iron oxyhydroxides, such as ferrihydrite or takovite (Marsh et al., 2013; Myagkiy et al., 2017). Therefore, the power of the light source should be adapted to avoid mineralogical transformation. This is one of the goals of the SOLSA project.

Concerning XRF or pXRF analyses, several factors influence the results (Hall et al., 2011, 2014, 2012; Laperche, 2005; Quiniou and Laperche, 2014; Ross et al., 2014a, 2014b). The surface state of the sample is important. Analyses on bulk samples give different results than those of powders, and of course glass beads in laboratory instruments. Powders are more homogeneous than drilled and polished samples, and thus present less scattered pXRF analyses (Figs. 6 to 9, and S2 to S5). For example, in the case of GN, the results are more variable among the bulk samples than in the powders (Figs. 8 and S4). This is linked to the heterogeneity and local mineral distribution in the bulk samples (e.g. Ca in calcite or gypsum, K in muscovite, Fe in hematite or Ti in rutile or anatase). Moreover, slight differences are highlighted for Si (every samples), Mg (SB and HG), Cr (SB and GN), Pb (GN), Zn (SB,

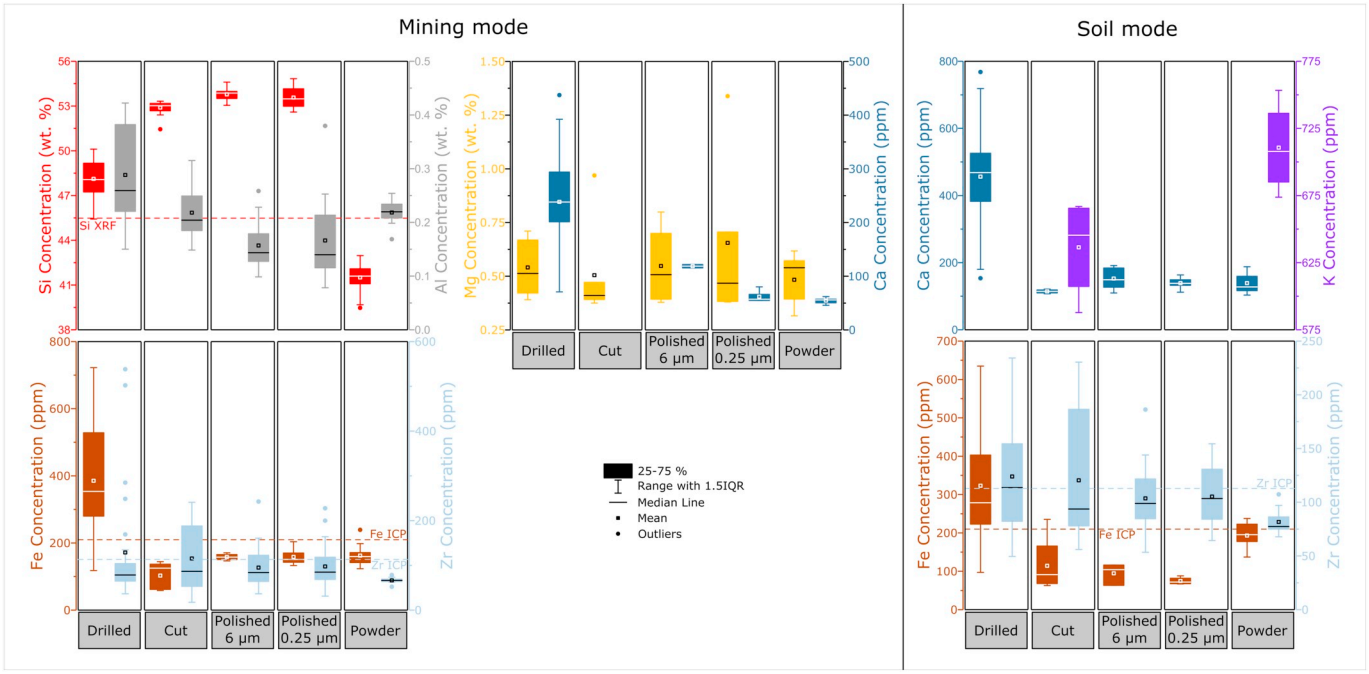

Fig. 6. Raw pXRF results for the SD sample (Si, Al, Mg, Ca, Fe, Zr, K).

HG and GN), Mn (SB and HG), Ni (HG) or Fe (HG) between rock surface and powder results. These differences may be related to the porosity of the powders, since they were not prepared as pellets. This sample surface thus leads to a decay of the signal. Another particular example is the SB sample. Analyses on powders gave higher metal contents than measured on drilled and polished samples (Fig. 7 and S3). SB is characterized by millimetric to centimetric pores on drilled and polished samples, and microporosity on powdered samples (Fig. 1d).

Comparing the results of the different surface states of the bulk samples (Figs. 6 to 9 and S2 to S5), polishing does not influence the results for most of the elements. This implies that analysing clean drill core surfaces will give coherent and reliable results. For on-line, real-time analyses, the porosity of the surface needs to be considered. The SOLSA expert system will be equipped with a profilometer to analyse the surface, intelligent software will indicate porosities such as holes, fractures and cracks so that erroneous results can be discarded.

4.2. Grain size effects on pIR analyses

Grain size effects on the analyses are known to be important to correctly interpret hyperspectral signals (Clark, 1999; Salisbury, 1991). The latter authors showed that grain size effects can even invert the longwave infrared spectra in the case of samples < 75 µm grain size. Concerning our samples, the major mineralogy of GN, SB, SD cannot be detected in the VNIR-SWIR region (quartz, feldspars). Only clay minerals (e.g. kaolinite), muscovite and/or biotite (GN) and oxyhydroxides as minor and accessory phases will be detected. Clay minerals and iron oxyhydroxides have micrometric sizes (fraction sizes ≤ 0.002 mm) typical for Ni-laterites. Therefore, calibration of the SOLSA instruments needs to be performed with clay fraction size materials. Laterites also host colloid-size materials (< 1000 nm; silica, poorly crystalline Fe-oxyhydroxides and clays), which need to be calibrated accordingly. SH, which is composed of Mg-Fe-Si-bearing minerals (serpentine, forsterite, enstatite, minor talc and microquartz), will give a pIR signal only for serpentine and talc. These minerals also belong to the clay fraction, which may impact the SWIR spectra.

4.3. Grain size and heterogeneous mineral distribution effect on pXRF analyses

The grain size effect and heterogeneous mineral distribution on pXRF results are however more important, as the SOLSA expert system targets qualitative but also semiquantitative results.

SD and SB are mainly composed of quartz (according to XRD, Fig. 3). This is supported by the mean Si concentration of 45 wt% after calibration from laboratory analyses (detailed in part 4.4., Figs. 11, 12, S6 and S7). However, the homogeneous SD shows a lower scattering (5% at maximum) than the porous SB for Si concentration (up to 15%). Moreover, the coarse-grained GN, with Si present in different minerals such as quartz and feldspar, shows a large scattering for this element (13% for a mean value of 31–33 wt%; Figs. 13 and S8) and the medium-grained HG shows a small Si deviation (around 3% for a mean value of about 17 wt%; Figs. 14 and S9). The same observation is made for other elements (Fe, Ca). In SB, the Ni content is heterogeneous and locally reaches an economic value of up to 1.1 wt% (Figs. 12 and S7). In this sample, Ni is hosted in clay-size minerals filling secondary millimetre-size veins. These veins can be easily missed during core scanning. However, the RGB camera and the profilometer will record the presence of greenish, soft Ni clay fills in veins crosscutting the harder quartz matrix of SB. These clay mixtures are also called garnierite. In contrast, the HG, representing the protolith of the nickel laterite, hosts 0.1–0.2 wt% Ni (Figs. 14 and S9). Nickel is present as a trace element in the major silicates (relict olivine and orthopyroxene, serpentine) in several hundreds and thousands of ppm, resulting in a low scattering of the results. These observations are in accordance with that of Hall et al. (2016, 2012) who showed that in coarse-grained samples, the concentration of elements had poor precision. Another factor to consider is the critical penetration depth (CPD (Potts and Webb, 1992)). The CPD corresponds to the depth in the sample beyond which fluorescence X-ray photons are absorbed and cannot be detected. The CPD varies depending on the atomic number of the elements (Z) hosted in the mineral, the heavier the elements, the deeper the CPD. For a silicate powder pellet with an assumed density of 2.1 $kg{\cdot}m^{-3}$, the CPD for Si Kα, Ca Kα and Fe Kα are 0.013, 0.036 and 0.18 mm, respectively (Potts and Webb, 1992). Thus, Hall et al. (2011) explained that due to the greater volumes of samples analysed for heavier elements, the pXRF analysis may not reflect the true composition if the sample is not homogeneous. Hall et al. (2012)

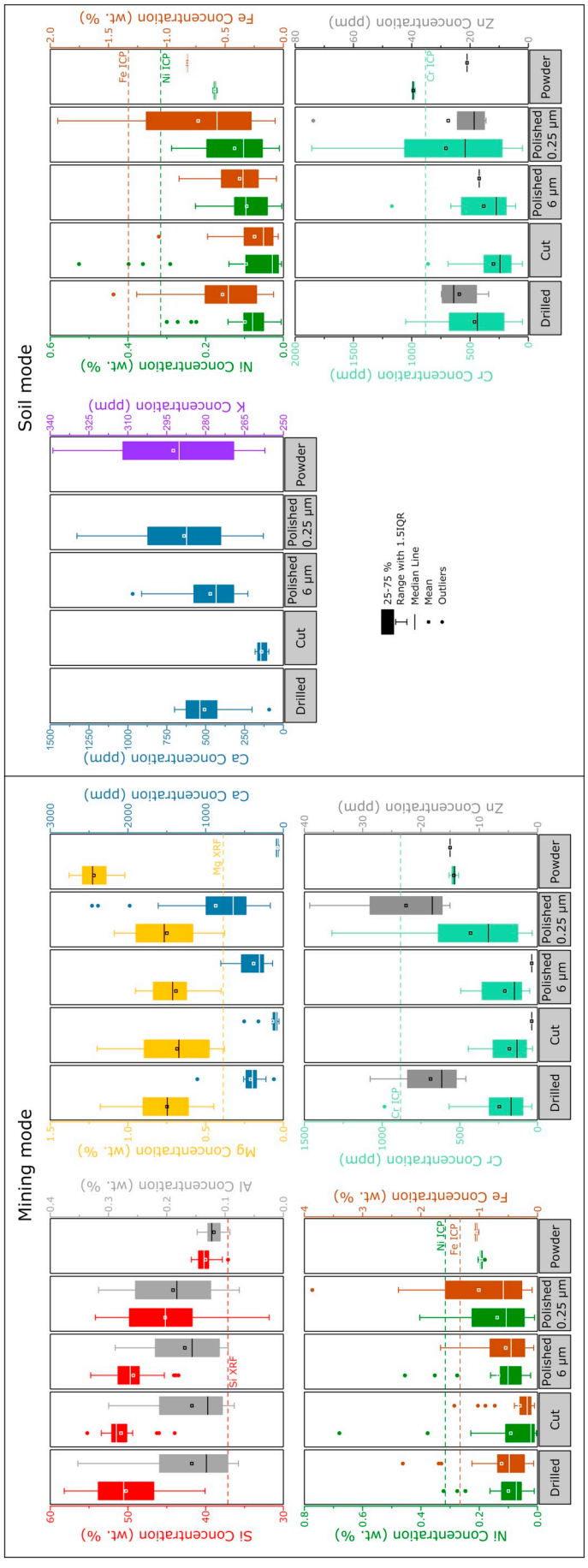

Fig. 7. Raw pXRF results for the SB sample (Si, Al, Mg, Ca, Ni, Fe, Cr, Zn, K).

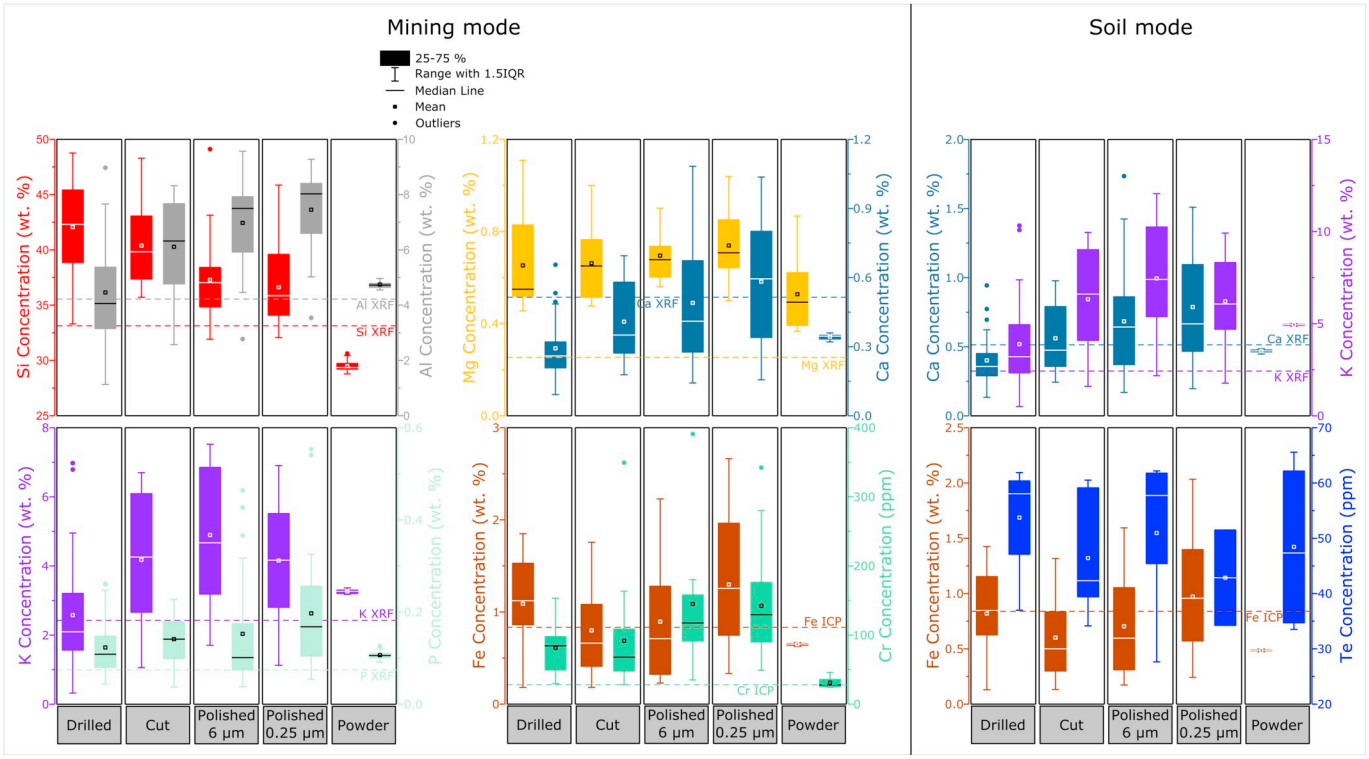

Fig. 8. Raw pXRF results for the GN sample (Si, Al, Mg, Ca, K, P, Fe, Cr, Te).

performed 1 to 15 measurements on the same samples and compared the deviation from the mean value (Figs. 4.1 to 4.4 in Hall et al., 2012). The authors stated that the error decreases drastically between 1 and 5 measurements, while it is less marked from 6 to 15 analyses.

For this study, we performed 26 measurements per analysis mode so 52 analyses per sample to enhance statistical reliability. We achieve the same order of deviation for bulk samples with 20 measurements per mode for HG and GR, and 15 per mode for SD and SB. In the case of the more homogeneous powders, the minimum number of measurements required per mode is 8. Some examples are presented in Fig. S10, but the same behaviour is observed for all results. Our study confirms that the texture and mineralogical heterogeneity clearly influences the scattering of the results (Hall et al., 2011; Hall et al., 2012).

4.4. Calibration and the problem of light element analyses by pXRF

Furthermore, calibration of the instrument is a major issue. Figs. 6 to 9 and S2 to S5 illustrate that the results obtained by pXRF are often different from those obtained by benchtop XRF or ICP. The perfect example of the calibration issue concerns Si in sandstone (SD), a sample composed of almost pure quartz. Without calibration of our instrument with our own reference sample set, the pXRF analysis on bulk samples indicates about 53 wt% of Si except for the drilled sample with a value of about 48 wt% (Figs. 6 and S2). However, the theoretical value in the case of pure quartz (i.e. without other elements or minerals) is around 47 wt%. The same analysis for the powder indicates a mean value of about 41 wt%, This is clearly below the theoretical value (Figs. 6 and S2). It is also worth noting that a clear difference between powder and bulk results is often observed in our pXRF measurements (Si, K, Sr, Zr, Fe, Mg, Ca, Ni, S, Cr, Mn, V, Al, Cl, Zn, Ba, As, Ti, Rb, Nb, Sn, Pb, Figs. 6 to 9 and S2 to S5).

Based on our observations, since powder results differ from those of the bulk samples, we suggest two types of calibration: (i) on powders and (ii) on bulk samples. These calibrations, performed on reference samples previously analysed by benchtop XRF and thus perfectly known, should take into account the whole range of concentrations for the elements analysed. Then, by comparing laboratory measurements with pXRF values obtained on bulks and powders for these reference samples, two calibration curves can be plotted. This allows re-calculating the real values for the unknown samples.

Applying these calibrations on our measurements, better results are achieved (e. g. Si, Ni for SB; Si, Zn, Ca, Zr for GN; Mg, Ca, Zn, Cr for HG and Si, Sr for SD) (Figs. 11 to 14 and S6 to S9). Comparing our calibrated pXRF results with those of laboratory XRF and ICP-AES, significant differences are still noted. The results of pXRF are not systematically higher or lower. Our study shows that: (1) Calibration with target material is mandatory, (2) that a XRF line drill core scan can be taken only as a qualitative indicator.

Furthermore, pXRF spectrometers are not recommended for analysing light elements (i.e. Mg, Si, Al) due to the important error. Fig. 15 shows examples of Mg and Si content determination in our samples. High Mg contents such as present in HG have a low error (5%), while low Mg contents exhibit an error of the same order as the value (94.4%). For our on-line analyses on Ni-laterite drill cores, we can use the Mg values as an indicator, as Mg drastically drops towards the top of the laterite profile from > 10 wt% to < 1 wt% in the so-called Mg discontinuity (Butt and Cluzel, 2013; Fritsch et al., 2014). Indeed, a 100% uncertainty on a 1 wt% concentration gives a range of concentration between 0 and 2 wt%. This is still far enough from the higher Mg concentrations (10 wt%) measured at the base of Ni-laterite profile to be discriminant for the ROI definition. In the same way, Si drops drastically in the yellow and red laterite horizons from several tens of percent to below 5%, providing a sufficient contrast for ROI definition.

For the SOLSA expert system ID A, one single measurement, as a line scan on drill cores can only be taken as a qualitative indication to define regions of interests to be further analysed by SOLSA ID B benchtop device.

4.5. Instrumental evaluation for the on-site combined analytical benchtop system

The SOLSA ID B benchtop system combines XRD-XRF, Raman and IR spectroscopies. In this study, we performed laboratory Raman spectroscopy and X-Ray Powder Diffraction.

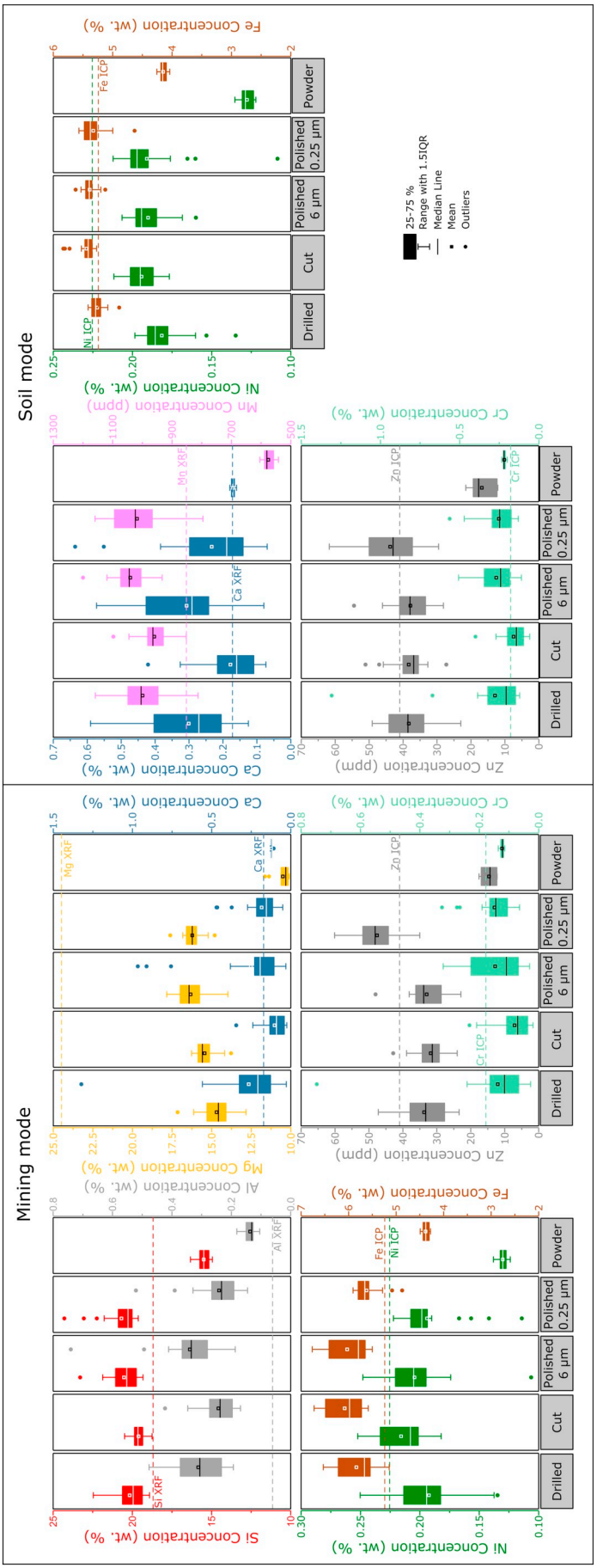

Fig. 9. Raw pXRF results for the HG sample (Si, Al, Mg, Ca, Ni, Fe, Zn, Cr, Mn).

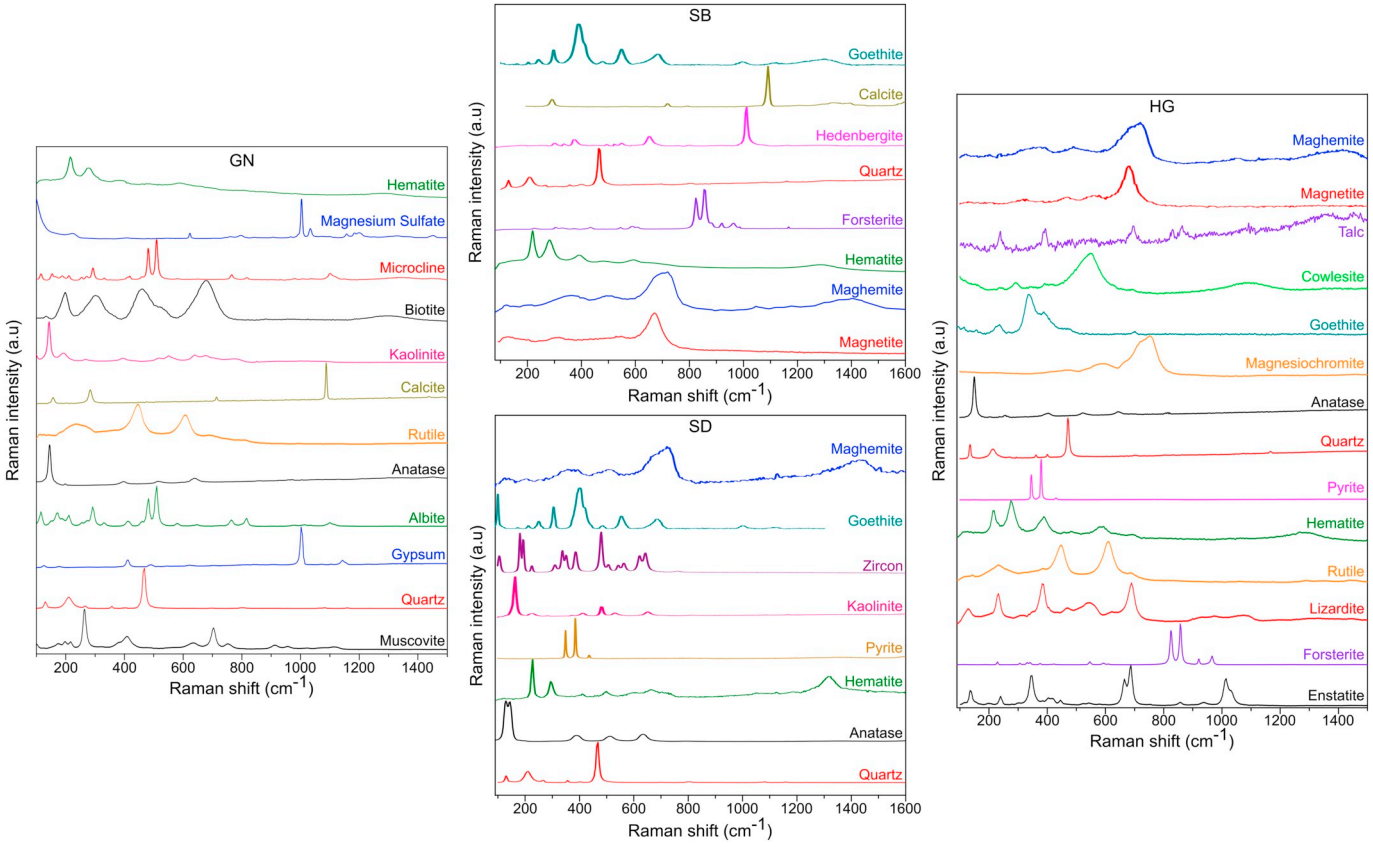

Fig. 10. Raman spectra collected on the bulk samples.

Raman spectroscopy was performed on powders (< 80 μm) and bulk samples using a 10 μm and 0.8 μm beam, respectively. The large beam size on powder samples gives an accurate major mineral composition for SD, SB and HG, but appears limited in the case of GN (Fig. 4). In GN, quartz was detected as major mineral while the feldspars (about 50%) appear as small peaks just above the background and is difficult to identify. However, microbeam spot analyses allow a more accurate study of the samples by enhancing the number of minerals detected (Table 2). Our results are compared with those of Secchi et al. (2018), who also analysed HG and SB. The authors used different configurations: 633, and 785 nm with a beam of 3–5 μm diameter. The results are comparable (Table 2) as they found lizardite and goethite,

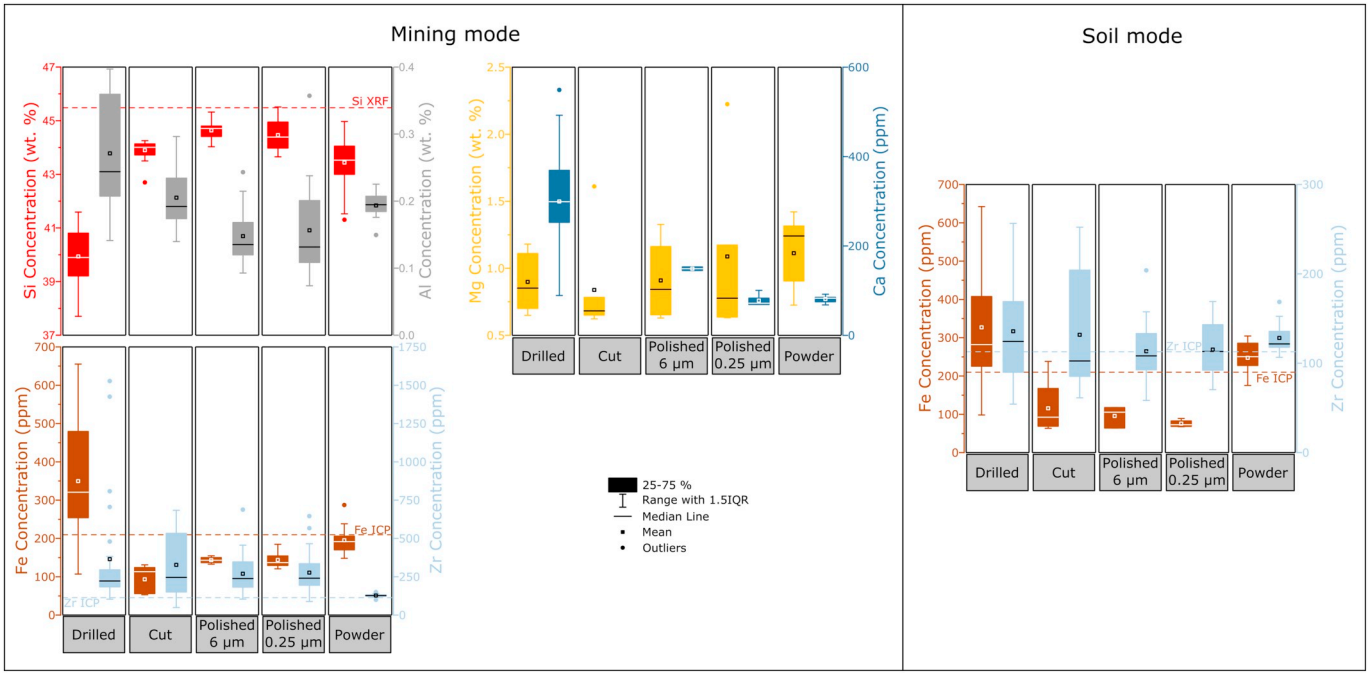

Fig. 11. Calibrated pXRF results for the SD sample (Si, Al, Mg, Ca, Fe, Zr).

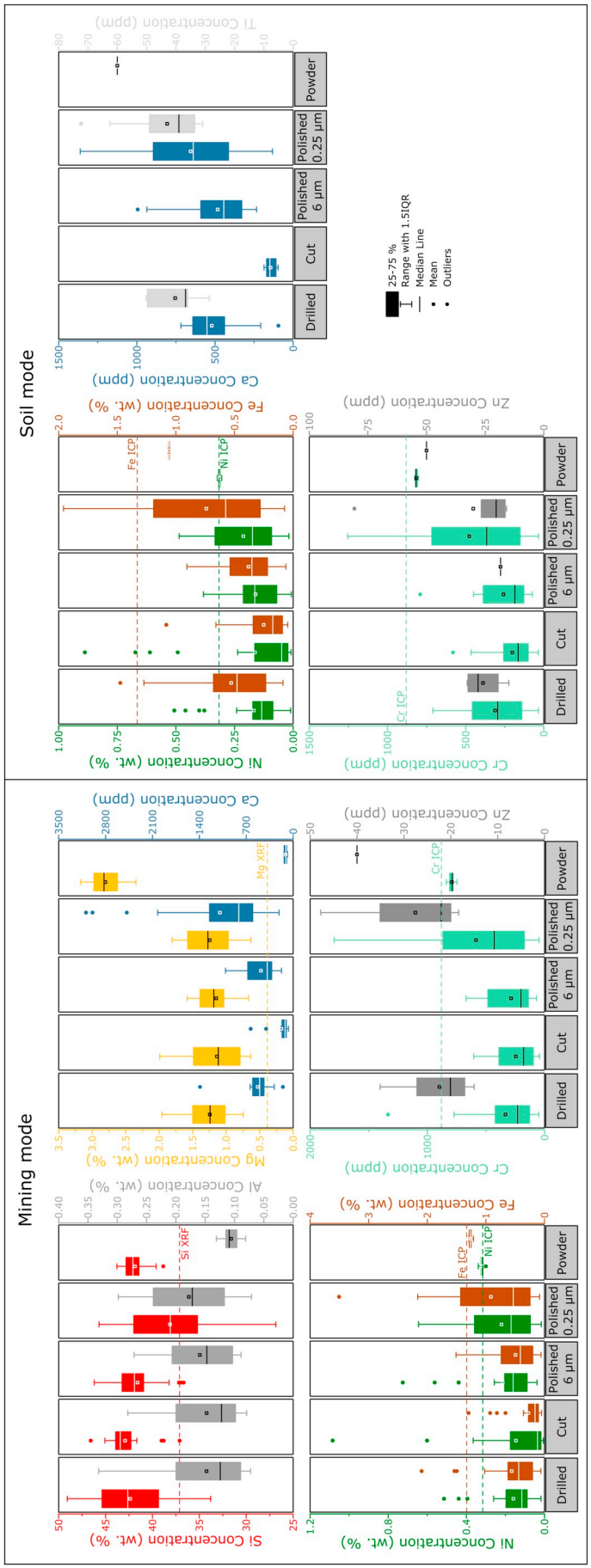

Fig. 12. Calibrated pXRF results for the SB sample (Si, Al, Mg, Ca, Ni, Fe, Cr, Zn, Ti).

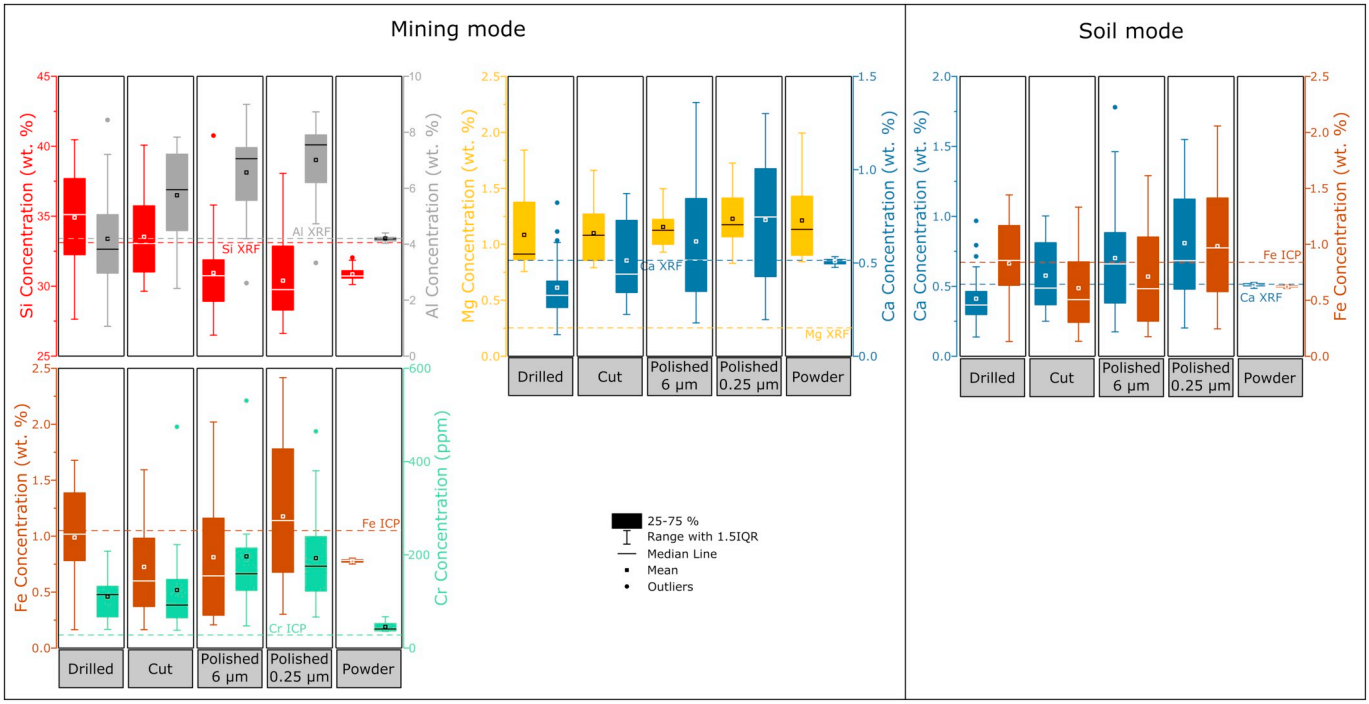

Fig. 13. Calibrated pXRF results for the GN sample (Si, Al, Mg, Ca, Fe, Cr).

magnesiochromite, talc, quartz, cowlesite (zeolite, $Ca(Al_2Si_3O_{10}(H_2O))$ and dwornikite ($(Ni, Fe)SO_4(H_2O)$)).

A prior evaluation of using Raman Spectroscopy on the SOLSA ID A system is hindered to the time-consuming Raman analyses (60 to 100 s per analysed region). This is too long for an on-line real-time analysis with a target amount of drill cores of up to 80 m per day. For that reason, Raman spectroscopy is combined in the offline benchtop analytical system. For the combined Raman-XRF-XRD (benchtop) analyses, powder analyses are recommended to avoid erroneous results related to heterogeneity.

4.6. Implication for the SOLSA ID A online real-time expert system

Our results show that the combination of analytical techniques is necessary in order to gather the maximum of information from one sample. Each technique has its own advantages and drawbacks depending on its physical characteristics. Only the combined analytical approach can overcome these drawbacks. However, a univocal characterization of the rocks cannot be achieved without an accurate calibration of the instruments on representative target materials. Therefore, it is strongly recommended that for each mining application, typical reference samples need to be fully characterized by laboratory instruments to validate and calibrate the on-line expert systems. Even if reference samples such as white and black Teflon are used to calibrate the VNIR-SWIR cameras, this calibration does not take into account the grain size and specific mineral associations or mineral chemistries, which are specific for laterite, and drastically differ from those for e.g. gold deposits.

For pXRF, it is recommended to calibrate with materials covering the whole range of concentrations for the major and minor elements to be analysed and the different rock textures that are present in the target material in order to define the possible elemental range for the samples.

For on-line and real-time analyses on drill cores, it is important to achieve rapid segmentation and selection of regions of interest. In the case of Ni laterites, Mg, Si, Fe and Ni contribute to the segmentation with significant positive and negative anomalies along the profile: high Mg and Si (around 10–15% and 15–20% respectively) in the lower part (saprolite and protolith); high Fe (40–60%) in the upper horizons and high to medium Ni contents in the saprolite and above located yellow limonite horizons (Orberger et al., 2016; Tauler et al., 2017).

SOLSA ID A will be equipped with VNIR and SWIR Specim cameras. This range covers most of the minerals to be targeted in Ni laterite ores, associated siliceous breccias and protolith, serpentinized harzburgite or dunite. VNIR will add to the chemical segmentation the detection of iron-oxyhydroxides in the upper horizon, and SWIR will contribute with the detection of swelling and non-swelling clays in the downward laterite profile or along drained zone. The SOLSA SWIR camera will differentiate between clays (e.g. nontronite, saponite) and serpentine (e.g. lizardite). Smart algorithms will perform a mapping (and quantitative evaluation of serpentine and clays). The increase of serpentine and the appearance of olivine and pyroxene will be indicative for the transition from saprolite to the serpentinized peridotite (protolith). In addition, SWIR detects Ni-rich clay, serpentine and talc mixtures (garnierite) present in hydrofractured rocks (HG, SB and saprolites, in this study up to 1 wt% Ni). These green phases will be additionally recorded by the RGB camera. Of course, VNIR and SWIR do not cover the significant bands of quartz and carbonates, and a compromise is to target these minerals indirectly by the XRF device (high Si and Ca). Using XRF and VNIR-SWIR on the same scanning device brings technical challenges. Indeed, each instrument analyses different volumes and/or areas, and these analyses are performed at different distances from the samples (close to surface for XRF, about 40 cm for hyperspectral cameras). For hyperspectral mapping (compared to point analyses), challenges are the accuracy of the texture and grain size definition (Bui et al., 2018).

Chemical and mineral analyses by SOLSA ID A will be supported by a high resolution RGB camera, to define the major segments and ROIs. Imaging gives the major information on colour, fractures, cracks and rock textures. For Ni laterites, calibration particularly in the red, green

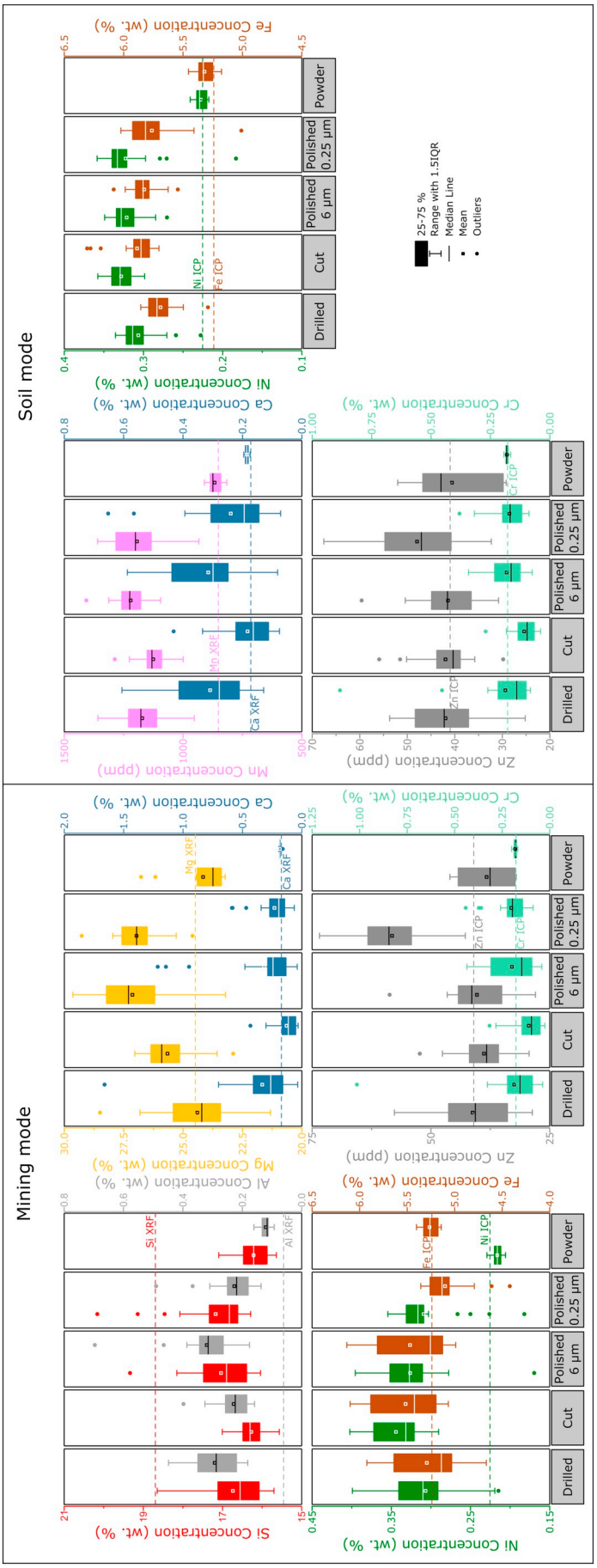

Fig. 14. Calibrated pXRF results for the HG sample (Si, Al, Mg, Ca, Ni, Fe, Zn, Cr, Mn).

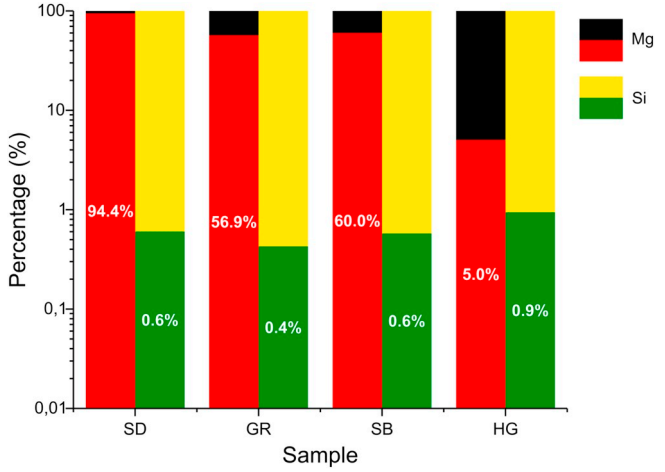

Fig. 15. Histogram presenting the percentage of the mean error in comparison to the mean concentration for Mg (error in red) and Si (error in green) for the four samples. (For interpretation of the references to in this figure legend, the reader is referred to the web version of this article.)

and brown colours must be performed, taking into account that both Fe-oxyhydroxydes and Ni-bearing serpentines (forming the bulk of the saprolite horizon) may look brown with the naked eye. As soil facies, in particular in the upper part of the laterite profile, are very fine grained, a reference sample library of the facies will be established.

Heterogeneities, in particular the presence of clasts and concretions, will be part of the facies record. Textures such as empty fractures, cracks and negative crystal/particle shapes will be recorded contemporaneously by profilometry.

5. Conclusions

This study on rocks of contrasting textures, chemistry, mineralogy at different surface states shows the importance of a multi-technique approach for systematic, simultaneous mineralogical and chemical drill core scanning. By focusing on portable Infra-red spectroscopy and handheld X-Ray Fluorescence in mining and soil mode, on powders and bulk samples, we demonstrated that the surface state of the rock has a minor effect on the signals gathered by the above-mentioned techniques. Therefore, clean drilled surface can be analysed avoiding a supplement step of core cutting, a common practice. The lower accuracy of scanning devices compared to laboratory instruments and the low statistics of analyses during core scanning present a compromise to quickly define regions of interest. The combination of XRF-VNIR-SWIR supported by RGB cameras and profilometers compensates higher detection limits of elements, the analyses of well-defined target minerals and the low number of analyses. Thus, the SOLSA ID A device, containerized, robotized and semiautomatized, targets ROI definition on up to 80 m drill core per day. Powerful software under development will lead to real time geomodel updating, implying near-real time decision making.

However, a precise calibration on ore, even better, mine specific reference samples, is mandatory, especially for the XRF device since this method depends on density, sample heterogeneity, porosity, or presence of air between the sample and the detector. XRF on this scanning device will give qualitative results (high or low).

Finally, a reliable analysis requires the development of a mineral library adequate to the specific characteristics of the ore and mine to be analysed. This database should be comprehensive for Raman, XRD and hyperspectral data. In this optic, a part of the SOLSA project is dedicated to the development of a Raman Open Database (ROD) and a Hyperspectral Open Database (HOD), which will be connected to the already existing Crystallographic Open Database (COD).

Table 2
List of all the minerals detected during this study and comparison with the study of (Secchi et al., 2018). XRD: X-ray Diffraction, Rp: Raman spectroscopy on powders, Rs: Raman spectroscopy on bulk samples, Rr: Raman spectroscopy performed in the study of Secchi et al. (2018), pIR: portable Infrared spectroscopy, Mn: Montmorillonite.

	SD				SB					GN				HG				
	XRD	Rp	Rs	pIR	XRD	Rp	Rs	Rr	pIR	XRD	Rp	Rs	pIR	XRD	Rp	Rs	Rr	pIR
Quartz	X	X	X		X	X	X	X		X	X	X				X	X	
Moganite								X										
Zircon			X															
Albite										X	X	X						
Biotite												X						
Feldspar										X	X	X						
Muscovite										X		X						
Chlorite										X								
Illite				X						X			X					
Kaolinite												X		X				
Forsterite							X								X	X	X	
Enstatite														X		X	X	
Hedenbergite							X											
Lizardite/chrysotile														X	X	X	X	X
Talc														X		X	X	
Cowlesite (zeolite)																X	X	
Dwornikite																	X	
Smectite				Mn														
Magnetite							X											
Magnesiochromite																X	X	
Maghemite							X											
Hematite			X	X	X		X	X				X	X			X		
Goethite					X			X	X							X	X	
Rutile												X				X		
Anatase			X									X				X		
Pyrite			X													X		
Gypsum												X						
Calcite							X					X						
Magnesium sulphate												X						

Supplementary data to this article can be found online at https://doi.org/10.1016/j.gexplo.2018.12.010.

Acknowledgements

We thank the European Commission for having sponsored this study in the frame of the SOLSA project (H2020 program): SC5-11d-689868. We also thank M. Alleki (BRGM/LAB/MIN) for careful sample preparation, and the BRGM/LAB/ENV Inorga team for the ICP-AES and XRF laboratory analyses. Finally, we thank the three reviewers for the constructive and interesting remarks and comments on this paper.

References

Braibant, L., Barnabé, P., Leroy, S., Dislaire, G., Pirard, E., 2018. Non-ferrous scrap metals classification by hyperspectral and multi-energy X-ray transmission imaging. In: Verlag, S. (Ed.), 8th Sensor-based Sorting & Control. Aachen, The Netherlands, pp. 39–47.

Bui, T., Orberger, B., Blancher, S., Mohammad-Djafari, A., Pillière, H., Salaün, A., Bourrat, X., Maubec, N., Lefèvre, T., Rodriguez, C., Vaitkus, A., Grazulis, S., Duée, C., Harang, D., Wallmach, T., El Mendili, Y., Chateigner, D., Buxton, M., Le Guen, M., 2018. Building a Hyperspectral Library and Its Incorporation Into Sparse Unmixing for Mineral Identification, IGARSS 2018, Valencia, Spain.

Butt, C.R.M., Cluzel, D., 2013. Nickel laterite ore deposits: weathered serpentinites. Elements 9, 123–128.

Cathelineau, M., Myagkiy, A., Quesnel, B., Boiron, M.C., Gautier, P., Boulvais, P., Ulrich, M., Truche, L., Golfier, F., Drouillet, M., 2017. Multistage crack seal vein and hydrothermal Ni enrichment in serpentinized ultramafic rocks (Koniambo massif, New Caledonia). Mineral. Deposita 52, 945–960.

Chang, Z.S., Yang, Z.M., 2012. Evaluation of inter-instrument variations among Short Wavelength Infrared (SWIR) devices. Econ. Geol. 107, 1479–1488.

Clark, R.N., 1999. Spectroscopy of Rocks and Minerals and Principles of Spectroscopy. John Wiley & Sons, New York, NY.

Cudahy, T., Hewson, R., Caccetta, M., Roache, A., Whitbourn, L., Connor, P., Coward, D., Mason, P., Yang, K., Huntington, J., Quigley, M., 2009. Drill core logging of plagioclase feldspar composition and other minerals associated with Archean gold mineralization at Kambalda, Western Australia, using a bidirectional thermal infrared reflectance system. Rev. Econ. Geol. 16, 223–235.

Duke, E.F., Lewis, R.S., 2010. Near infrared spectra of white mica in the Belt Supergroup and implications for metamorphism. Am. Mineral. 95, 908–920.

Fritsch, E., Juillot, F., Dublet, G., Fandeur, D., Fonteneau, L., Martin, E., Auzente, A.L., Morin, G.R.J.L., Galoisy, L., Calas, G.G.O., Boulvais, P., Cathelineau, M., Caner, L., Beaufort, D.P.S., 2014. Analyse fine de minerais latéritiques (approches pétrographique, minéralogique, géochimique et isotopique). In: CNRT Nickel & Son Environnement, pp. 131.

Gomez Laserna, O., 2015. Development of In Situ Non Destructive Analytical Methodologies for the Conservation Diagnosis of Urban Built Heritage. Universidad del País Vasco - Euskal Herriko Unibertsitatea, Spain.

Haavisto, O., Kauppinen, T., Häkkänen, H., 2013. Laser-induced breakdown spectroscopy for rapid elemental analysis of drillcore. IFAC Proc. Vol. 46, 87–91.

Haest, M., Cudahy, T., Laukamp, C., Gregory, S., 2012. Quantitative mineralogy from infrared spectroscopic data. I. Validation of mineral abundance and composition scripts at the Rocklea Channel iron deposit in western Australia. Econ. Geol. 107, 209–228.

Hall, G., Buchar, A., Bonham-Carter, G., 2011. Quality Control Assessment of Portable XRF Analysers: Development of Standard Operating Procedures, Performance on Variable Media and Recommended Uses - Phase I. Canadian Mining Industry Research Organization (CAMIRO) exploration Division.

Hall, G.E.M., Page, L., Bonham-Carter, G.F., 2012. Quality Control Assessment of Portable XRF Analysers: Development of Standard Operating Procedures, Performance on Variable Media and Recommended Uses - Phase II. Canadian Mining Industry Research Organization (CAMIRO) Exploration Division.

Hall, G.E.M., Bonham-Carter, G.F., Buchar, A., 2014. Evaluation of portable X-ray fluorescence (pXRF) in exploration and mining: phase 1, control reference materials. Geochem. Explor. Environ. Anal. 14, 99–123.

Hall, G.E.M., McClenaghan, M.B., Page, L., 2016. Application of portable XRF to the direct analysis of till samples from various deposit types in Canada. Geochem. Explor. Environ. Anal. 16, 62–84.

Hu, B.F., Chen, S.C., Hu, J., Xia, F., Xu, J.F., Li, Y., Shi, Z., 2017. Application of portable XRF and VNIR sensors for rapid assessment of soil heavy metal pollution. PLoS One 12, 13.

Kristova, P., Hopkinson, L., Rutt, K., Hunter, H., Cressey, G., 2013. Quantitative analyses of powdered multi-minerallic carbonate aggregates using a portable Raman spectrometer. Am. Mineral. 98, 401–409.

Laperche, V., 2005. Evaluation des performances du spectromètre portable de fluorescence X Niton XL723S (au laboratoire et sur le terrain). BRGM.

Liritzis, I., Zacharias, N., 2011. Portable XRF of archaeological artifacts: current research, potentials and limitations. In: Shackley, M.S. (Ed.), X-ray Fluorescence Spectrometry (XRF) in Geoarchaeology. Springer New York, New York, NY, pp. 109–142.

Lutterotti, L., Matthies, S., Wenk, H.R., Schultz, A.S., Richardson, J.W., 1997. Combined texture and structure analysis of deformed limestone from time-of-flight neutron diffraction spectra. J. Appl. Phys. 81, 594–600.

Lypaczewski, P., Rivard, B., Gaillard, N., Perrouty, S., Linnen, R.L., 2017. Hyperspectral characterization of white mica and biotite mineral chemistry across the Canadian Malartic gold deposit, Québec, Canada. In: 14th SGA Biennial Meeting, Quebec City, Canada, pp. 1095–1097.

Marsh, E., Anderson, E., Gray, F., 2013. Nickel-cobalt laterites; a deposit model. Sci. Investig. Rep. 38.

Myagkiy, A., Truche, L., Cathelineau, M., Golfier, F., 2017. Revealing the conditions of Ni mineralization in the laterite profiles of New Caledonia: insights from reactive geochemical transport modelling. Chem. Geol. 466, 274–284.

Nguegang Kamwa, B., Laflamme, M., Constantin, M., Rifai, K., Castello, M., Fytas, K., 2017. Definition of a sampling strategy by statistical analyses of LIBS data in the context of portable gold analyzer. In: 14th SGA Biennal Meeting, Québec City, Canada, pp. 155–158.

Orberger, B., Duée, C., Salaün, A., Rodriguez, C., 2016. Handheld XRF Analyses on the Drill Core 11MC (Ni-laterite, New Caledonia), Internal Report.

Pérez-Barnuevo, L., Lévesque, S., Bazin, C., 2018. Automated recognition of drill core textures: a geometallurgical tool for mineral processing prediction. Miner. Eng. 118, 87–96.

Portable XRF Services, 2016. Detecting the Primary Lithology in Regolith Using pXRF and TerraSpec (VNIR-SWIR) Results.

Potts, P.J., Webb, P.C., 1992. X-ray-fluorescence spectrometry. J. Geochem. Explor. 44, 251–296.

Quiniou, T., Laperche, V., 2014. An assessment of field-portable X-ray fluorescence analysis for nickel and iron in laterite ore (New Caledonia). Geochem. Explor. Environ. Anal. 14, 245–255.

Roache, T.J., Walshe, J.L., Huntington, J.F., Quigley, M.A., Yang, K., Bil, B.W., Blake, K.L., Hyvärinen, T., 2011. Epidote–clinozoisite as a hyperspectral tool in exploration for Archean gold. Aust. J. Earth Sci. 58, 813–822.

Ross, P.S., Bourke, A., Fresia, B., 2013. A multi-sensor logger for rock cores: Methodology and preliminary results from the Matagami mining camp, Canada. Ore Geol. Rev. 53, 93–111.

Ross, P.S., Bourke, A., Fresia, B., 2014a. Improving lithological discrimination in exploration drill-cores using portable X-ray fluorescence measurements: (2) applications to the Zn-Cu Matagami mining camp, Canada. Geochem. Explor. Environ. Anal. 14, 187–196.

Ross, P.S., Bourke, A., Fresia, B., 2014b. Improving lithological discrimination in exploration drill-cores using portable X-ray fluorescence measurements: (1) testing three Olympus Innov-X analysers on unprepared cores. Geochem. Explor. Environ. Anal. 14, 171–185.

Salisbury, J.W., 1991. Infrared (2.1–25 μm) Spectra of Minerals. Johns Hopkins University Press.

Secchi, M., Zanatta, M., Borovin, E., Bortolotti, M., Kumar, A., Giarola, M., Sanson, A., Orberger, B., Daldosso, N., Gialanella, S., Mariotto, G., Montagna, M., Lutterotti, L., 2018. Mineralogical investigations using XRD, XRF, and Raman spectroscopy in a combined approach. J. Raman Spectrosc. 49, 1023–1030.

Shackley, M.S., 2010. Is there reliability and validity in portable X-Ray Fluorescence spectrometry (pXRF)? In: The SAA Archaeological Record. Society for American Archaeology.

Shankar, V., 2015. Field Characterization by Near Infrared (NIR) Mineral Identifiers - A New Prospecting Approach. Global Challenges, Policy Framework & Sustainable Development for Mining of Mineral and Fossil Energy Resources (Gcpf2015) 11. pp. 198–203.

Streubel, L., Jacobsen, L., Merk, S., Thees, M., Rammlmair, D., Meima, J., Mory, D., 2016. Rapid analysis of geological drill-cores with LIBS. Optik Photonik 11, 23–27.

Tauler, E., Lewis, J.F., Villanova-De-Benavent, C., Aiglsperger, T., Proenza, J.A., Domenech, C., Gallardo, T., Longo, F., Gali, S., 2017. Discovery of Ni-smectite-rich saprolite at Loma Ortega, Falcondo mining district (Dominican Republic): geochemistry and mineralogy of an unusual case of “hybrid hydrous Mg silicate - clay silicate” type Ni-laterite. Mineral. Deposita 52, 1011–1030.

Tjallingii, R., Rohl, U., Kolling, M., Bickert, T., 2007. Influence of the water content on X-ray fluorescence core-scanning measurements in soft marine sediments. Geochem. Geophys. Geosyst. 8, 12.

Tukey, J.W., 1977. Exploratory Data Analysis.

Tykot, R.H., 2016. Using nondestructive portable x-ray fluorescence spectrometers on stone, ceramics, metals, and other materials in museums: advantages and limitations. Appl. Spectrosc. 70, 42–56.

Wells, M.A., Ramanaidou, E.R., 2015. Raman spectroscopic core scanning for iron ore and BIF characterization. In: Dong, F. (Ed.), Proceedings of the 11th International Congress for Applied Mineralogy (ICAM). Springer International Publishing, Cham, pp. 387–396.

Whitbourn, L., Huntington, J., Munday, T., Vearncombe, J., 2011. CSIRO's HyLogging™ systems; production proven technology for the exploration and mining sector. Bull. Australian Inst. Geosci. 54, 85–88.